

Synthesis and characterization of Zn/Fe layered double hydroxide and its composites for copper adsorption from aqueous solution

M.T. Amin^{a,b,*}, A.A. Alazba^{a,c}, M. Shafiq^a

^aAlamoudi Water Research Chair, King Saud University, P.O. Box: 2460, Riyadh 11451, Kingdom of Saudi Arabia, Tel. +966 114673737; Fax: +966 114673739; emails: mtamin@ksu.edu.sa (M.T. Amin), alazba@ksu.edu.sa (A.A. Alazba), msrana@ksu.edu.sa (M. Shafiq)

^bDepartment of Environmental Sciences, COMSATS Institute of Information Technology, Abbottabad 22060, Pakistan

^cAgricultural Engineering Department, King Saud University, P.O. Box: 2460, Riyadh 11451, Kingdom of Saudi Arabia

Received 8 January 2020; Accepted 13 December 2020

ABSTRACT

Application of zinc–iron layered double hydroxide (ZnFe-LDH) and its composites with single-wall carbon nanotubes (LDH/CNT) and biochar derived from orange peel biomass (LDH/OPb) for batch adsorption of Cu²⁺ was extensively studied. The X-ray diffraction (XRD) patterns and energy-dispersive X-ray (EDX) analyses confirmed some chemical changes and successful adsorption of Cu²⁺. An equilibrium contact time of 60 min was adopted for the optimum removal of the Cu²⁺ using all the adsorbents. LDH/OPb demonstrated a greater affinity for the Cu²⁺ than LDH/CNT and ZnFe-LDH due to its large surface area. The adsorption capacity decreased with increasing removal efficiency as the adsorbents dose increased from 0.2 to 0.9 g. However, both the adsorption capacity and removal efficiency increased as pH increased from 2.0 to 5.0 with an optimum pH of approximately 6.0. The removal efficiency decreased with a higher increase in the sorption capacity of LDH/OPb than other adsorbents as the initial Cu²⁺ concentration increased from 10 to 100 mg L⁻¹. The Langmuir model demonstrated a better estimation and a better fit to the adsorption data than the Freundlich and D–R isotherms. The pseudo-second-order kinetic model demonstrated the best fitting to the adsorption data compared with other kinetic models.

Keywords: Adsorption; Composites; Isotherms; Kinetics; Orange peel

1. Introduction

The surge in the discharge of heavy metals ions into the environment through natural and anthropogenic activities is threatening the global health of the ecosystem. Heavy metal ions are long-lasting, non-degradable, and toxic to living beings. Among the most problematic heavy metal ions, the elevated amounts of the copper cation (Cu²⁺) in freshwater reservoirs pose a serious health threat to the environmental ecosystem. Cu²⁺ is one of the prevalent metal ions in electrical and electroplating industries and is also extensively being discharged from the pulp, paper mills, and petroleum refineries [1]. These discharged effluents possess

very high concentrations of Cu²⁺ according to water quality standards which stipulate 1.3 mg L⁻¹ of Cu²⁺ [2]. Therefore, there is an urgent need to reduce the concentration of Cu²⁺ and other hazardous pollutants in industrial wastewater before been discharged into waterways or sewage systems to sure a safe environment and human health.

Different technologies for wastewater decontamination such as ion exchange, phytoextraction, membrane filtration, coagulation and flocculation, and chemical precipitation have been explored to remove Cu²⁺ from industrial wastewater [3–5]. However, most of these technologies have some inherent advantages and limitations in terms of their applications, operation cost, and average

* Corresponding author.

removal capacities [6]. Among the existing water remediation technologies, adsorption is considered the best due to its lower cost, higher removal efficiency, applicability to a wide range of contaminants, and simplicity in operation [7,8]. However, the selection of the most appropriate and efficient adsorbent material for the removal of a particular contaminant demands crucial scrutiny. Continuous and extensive efforts have been made to develop efficient and low-cost adsorbent materials, like biochar prepared from wastes of plant materials, for sustainable Cu^{2+} removal from different environmental contaminants.

The layered double hydroxides (LDHs) are highly ordered two-dimensional anionic clays and have attracted considerable attention of researchers in the last decades for the sorption capacity of heavy metals and other contaminants because of their high specific surface area, high pH buffering capacities, good thermal stability, reversibility of structure, and high adsorption capacities [9,10]. Nano-sized LDHs structural formula can be presented as $[\text{M}_{1-x}^{2+} \text{M}_x^{3+} (\text{OH})_2]^{x+} (\text{A}^{n-})_{x/n} \cdot y\text{H}_2\text{O}$, where M^{2+} represents divalent metal ions such as (Mg^{2+} , Zn^{2+} , Ni^{2+} , Co^{2+} , Ca^{2+} , and Fe^{2+}), M^{3+} trivalent metal ions such as (Al^{3+} , Mn^{3+} , Ga^{3+} , Fe^{3+} , and In^{3+}), and A^{n-} an intercalated anion such as NO_3^- , Cl^- , CO_3^{2-} , and SO_4^{2-} [2]. Part of the octahedral M^{2+} cations is isomorphously substituted by M^{3+} cations and the excessive positive charges generated by this substitution are compensated with the presence of anions in the inter-layer space [11]. There are several methods to synthesize LDHs such as hydrothermal reaction, rehydration, intercalation, co-precipitation, and pre-pillaring [12], and the most frequently used is the co-precipitation method. The efficiency of LDHs in removing Cu^{2+} ions from wastewaters has been reported by many researchers. For example, Sun et al. [13] investigated the performance of $\text{Fe}_3\text{O}_4/\text{MgAl-LDH}$ nanocomposites for the removal of Cu^{2+} and reported a maximum adsorption capacity of 64.66 mg g^{-1} . Yue et al. [14] also studied MgAl-Cl LDH for Cu^{2+} removal and they realized 163 mg g^{-1} adsorption capacity.

In recent years, scientists are trying to increase the efficiencies of LDHs by developing their composites with other carbonaceous materials. For instance, compositing LDHs with biochar and/or carbon nanotubes (CNTs) can improve the properties of LDHs resulting in higher sorption efficiencies. Biochar is a stable and high degree porous pyrogenic black carbon derived from the pyrolysis of carbon-rich materials under an oxygen-free environment. It is an excellent adsorbent in terms of its high surface area and high adsorption properties. There are abundant raw materials for biochar production such as agricultural residues, municipal solid waste materials, industrial wastes, and by-products as well as many other non-conventional materials such as papers, algae, bones, and waste tires [15]. 124.73 million metric tons of citrus are annually produced worldwide [16]. Its peel is an important by-product with a high content of lignin, cellulose, and hemicellulose [17]. Recycling of orange peel waste to produce biochar has a double remediation technique; reduction of surface pollution on one hand and water decontamination on the other. Likewise, CNTs demonstrate exceptional sorption capacities for a range of environmental contaminants due to their hollow and layered structure, thermal and chemical stabilities, large

surface area, and higher mechanical strength. However, the poor degradability and toxicity of CNTs as well as the removal of loaded CNTs are of important consideration. The removal of loaded CNTs using conventional methods is inefficient due to their micro-sized structure.

Therefore, we proposed that compositing the orange peel derived biochar or CNTs with LDHs would produce efficient and novel adsorbents for cost-effective and eco-friendly removal of Cu^{2+} ions from wastewater in waterways or sewage systems. Hence, the objectives of this study were to synthesis and characterization of ZnFe-LDH and its composites with CNT (LDH/CNT) and biochar prepared from the waste of orange peels (LDH/OPb) through co-precipitation method, investigation of the adsorption behavior for Cu^{2+} onto the synthesized adsorbents through equilibrium and kinetics sorption batches, and identification of the sorption mechanism using different isotherm models.

2. Materials and methods

2.1. Chemicals/reagents and ZnFe-LDH preparation

The stock solution of copper nitrate [$\text{Cu}(\text{NO}_3)_2 \cdot 2.5\text{H}_2\text{O}$; AR grade Merck, Germany] was prepared using ultrapure water (Milli-Q integral water dispenser, resistivity: $18 \text{ M}\Omega \text{ cm}^{-1}$) and diluted further to achieve the desired initial concentrations of Cu^{2+} as required in the different batch experiments. The pH was adjusted while preparing the LDH and its composites, the solution pH in the different batch experiments was adjusted using NaOH and HCl solutions and measured using a microprocessor-based pH meter (PHS-3CW, China). Also, iron(III) nitrate nonahydrate ($\text{Fe}(\text{NO}_3)_3 \cdot 9\text{H}_2\text{O}$) and zinc nitrate hexahydrate ($\text{Zn}(\text{NO}_3)_2 \cdot 6\text{H}_2\text{O}$) were employed to prepare the ZnFe-LDH with a $\text{Zn}^{2+}/\text{Fe}^{3+}$ ratio of 1:2 using a simple co-precipitation method. Both solutions were added to the distilled water at a constant pH of 10.0 and ammonia was added dropwise with vigorous stirring for about 30 min to form a precipitate.

2.2. Preparation of the biochar and composite adsorbents

Orange fruit peels were collected locally in Riyadh, Saudi Arabia, and used for the preparation of OPb. First, orange peel (OP) powder with an average particle size less than 0.5 mm was prepared by crushing the oven-dried (3 h at 70°C) biomass of cleaned and washed orange peels. Calcination of the OP powder was performed at 800°C for 3 h using a box furnace (Nabertherm, B-150, Germany) to obtain the OPb of average particle size in the range of 50–75 μm , which was then washed with distilled water to achieve a neutral pH and dried at 100°C for 12 h. Composites of ZnFe-LDH with OPb and COOH functionalized single-wall CNTs (D 1.5 L 1–5-COOH, NANO LAB) were prepared by adding 5.0 g and 5.0 mL of OPb and single-wall CNT solution, respectively, to 50 and 100 mL solutions of both 0.5 M $\text{Zn}(\text{NO}_3)_2 \cdot 6\text{H}_2\text{O}$ and 1 M $\text{Fe}(\text{NO}_3)_3 \cdot 9\text{H}_2\text{O}$, respectively. After the formation of the precipitate via co-precipitation method, the slurry was filtered and washed several times using deionized water to achieve the neutral pH and subsequently oven-dried at 70°C for 15 h.

2.3. Batch experimentation

An appropriate amount of LDH or its composites was added to the metal solution of Cu^{2+} with different initial concentrations in batch experiments to achieve the required dose of the adsorbent. Samples in conical flasks (100 mL) were agitated in a temperature-controlled shaker (Wise Cube orbital, Wisd., ThermoStable IS-20; Daihan Scientific Co., Ltd., South Korea) for the required time at 30°C and fixed speed of 220 rpm. 5 mL of the sample was analyzed for the residual metal ion concentration using flame atomic absorption spectrometry (FAAS, Thermo Scientific, ICE 3000 Series, Cambridge, United Kingdom) then filtered using $0.45\ \mu\text{m}$ sieves. The adsorption capacities at any time t (q_t , mg g^{-1}) and equilibrium (q_e , mg g^{-1}) were evaluated using Eqs. (1) and (2), respectively, while the percentage removal of Cu^{2+} (R , %) was calculated according to Eq. (3).

$$q_t = \left(\frac{C_0 - C_t}{m} \right) V \quad (1)$$

$$q_e = \left(\frac{C_0 - C_e}{m} \right) V \quad (2)$$

$$R = \left(\frac{C_0 - C_t}{C_0} \right) \times 100 \quad (3)$$

where C_0 , C_e , C_t are the initial, equilibrium, and variable time t solution concentrations of Cu^{2+} (mg L^{-1}), respectively, m denotes the mass of the adsorbent, that is, LDH or its composite (g), and V is the volume of the metal solution (L).

3. Results and discussion

3.1. Characterization of the ZnFe-LDH and its composites with CNT and OPb

3.1.1. Fourier transform infrared and powder X-ray diffraction analyses

The Fourier transform infrared (FTIR) spectra of ZnFe-LDH and its composites before and after adsorption of Cu^{2+} are presented in Figs. 1a and b. The intense broad transmittance bands observed around $3,300\text{--}3,400\ \text{cm}^{-1}$ were attributed to O–H stretching vibrations arising from metal-hydroxide groups and interlayer water molecules especially in ZnFe-LDH and LDH/CNT composites while the stretching vibrations almost vanished in LDH/OPb composite spectra [18]. The broadness of this region here may be due to hydrogen bridging [9]. Likewise, the sharp peak around $1,615\ \text{cm}^{-1}$ was also due to the hydrogen bonded layer hydroxyl group (H–O–H) of interlayer adsorbed water [19–21]. However, the intensity of the H-bonded hydroxyl group peak decreased gradually in the ZnFe-LDH composite with CNT and almost disappeared in the composite with OPb, indicating the reduction in numbers of hydroxyl groups. Therefore, the decreased band intensity of O–H groups around $3,300\text{--}3,400$ and $1,615\ \text{cm}^{-1}$ after compositing the OPb with CNTs could be due to surface

adsorption and diffusion of O–H into micro-pore structure of CNTs and OPb [22,23]. Further, the complete removal of O–H bands in the LDH/OPb was due to hygroscopic nature of OPb. The observed band at $1,417\ \text{cm}^{-1}$ in the spectra can be assigned as the ammonium (NH_4^+) ions which could be a residue from the ammonium hydroxide aqueous solution used to adjust the pH of the reaction media [24,25]. A band at $923\ \text{cm}^{-1}$ indicated metal–oxygen (Zn–O, Fe–O, or Zn–O–Fe) vibration modes of LDH which suggested chemical interaction occurrence [26,27].

After adsorption of Cu^{2+} as shown in Fig. 1b, the prominent stretching bands of the H–O–H groups at $1,615\ \text{cm}^{-1}$ shifted to $1,636$ and $1,632\ \text{cm}^{-1}$ in ZnFe-LDH and LDH/CNT composites, respectively, which could be due to the interaction of Cu^{2+} with hydroxyl ions. The band at $1,417\ \text{cm}^{-1}$ in ZnFe-LDH slightly shifted to $1,414\ \text{cm}^{-1}$ but disappeared in LDH composite with CNT after Cu^{2+} adsorption [24,25]. New bands at $1,131$ and $1,110\ \text{cm}^{-1}$ were introduced in the spectra of ZnFe-LDH (Cu^{2+}) and LDH/CNT (Cu^{2+}), respectively, suggesting metal (hydr)oxide (Fe–O and Fe–OH) stretching [28–30]. A band at $923\ \text{cm}^{-1}$ was ascribed as metal oxygen vibration (Zn–O, Fe–O, and Zn–O–Fe) was slightly shifted to $920\ \text{cm}^{-1}$ [22,30–32], which could be owing to the substitution of Fe or Zn metal with Cu^{2+} ions at O-containing functional group. Therefore, the FTIR spectra showed that CNTs and OPb were embedded in the LDH structure, and post-adsorption FTIR spectra exhibited successful loading of Cu^{2+} onto the synthesized adsorbents.

Powder X-ray diffraction (XRD) technique was employed to analyze the chemical interactions and surface changes of ZnFe-LDH and its composites after adsorption of Cu^{2+} (Figs. 2a and b). The sharp peaks appearing at $2\theta = 24.10^\circ$, 33.07° , 35.60° , 40.78° , 49.42° , 53.95° , 62.27° , and 63.94° , were attributed to ZnO and ZnFe_2O_4 [33,34]. The XRD pattern of ZnFe-LDH revealed good crystallinity compared to the composite with CNT and OPb. For the XRD patterns of ZnFe-LDH after adsorption of Cu^{2+} (Fig. 2b), the characteristic diffraction peaks at $2\theta = 24.25^\circ$, 33.13° , 35.67° , 40.85° , 49.39° , 54.00° , 62.30° , and 64.03° were slightly shifted from left to right compared to ZnFe-LDH before adsorption which indicates successful adsorption of Cu^{2+} on the LDH surface.

A strong broadband appeared at $2\theta = 30.00^\circ$ in the ZnFe-LDH with CNT and OPb after Cu^{2+} adsorption demonstrating an amorphous nature, and the changes in intensity revealed the formation of new compounds with Cu^{2+} . According to the results of the characteristic peaks, it can be deduced that Cu^{2+} infiltrated the layers of the adsorbent material, got adsorbed, and then exuded according to the material properties [35].

3.1.2. Field emission scanning electron microscopy and energy-dispersive X-ray analyses

The field emission scanning electron microscopy (FE-SEM) and energy-dispersive X-ray (EDX) images show the surface morphology and qualitative elemental analysis of LDH and its composites. The FE-SEM images of ZnFe-LDH before and after Cu^{2+} adsorption along with the EDX spectra are presented in Figs. 3a and b. The images of ZnFe-LDH before adsorption (Fig. 3a) revealed very small irregular flakes and plates-like structures of different sizes,

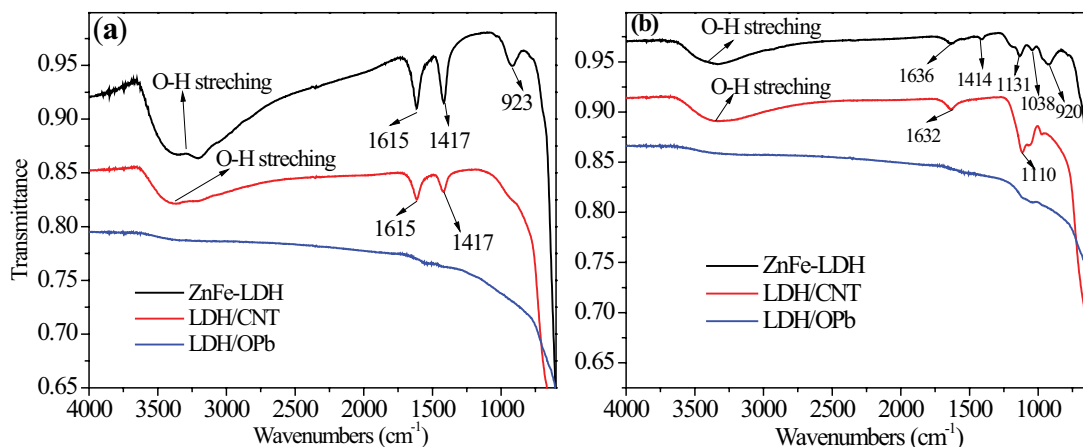


Fig. 1. FTIR spectra recorded for ZnFe-LDH, LDH/CNT, and LDH/OPb (a) before and (b) after the adsorption of Cu^{2+} .

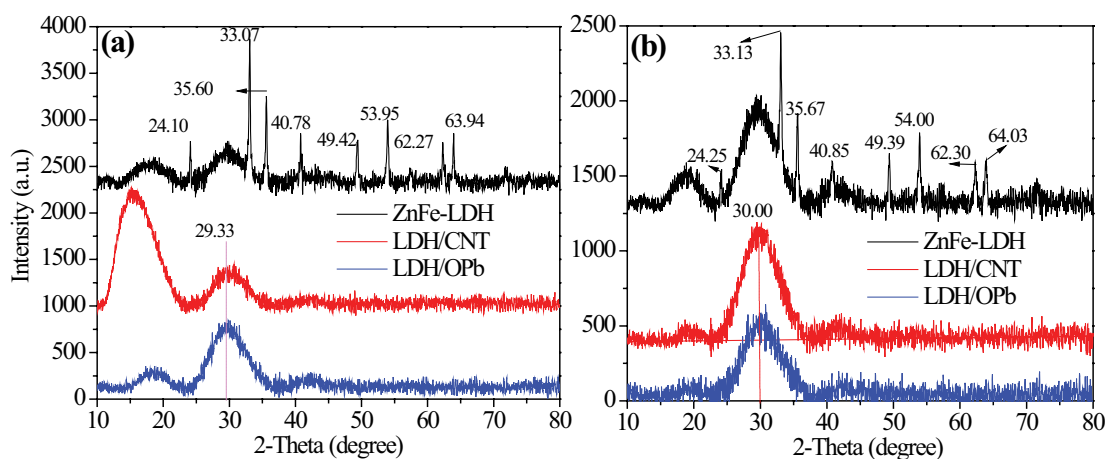


Fig. 2. XRD spectra recorded for ZnFe-LDH, LDH/CNT, and LDH/OPb (a) before and (b) after the adsorption of Cu^{2+} .

while whitish spots on the surface of the ZnFe-LDH were evident after Cu^{2+} adsorption which was attributed to the adsorbed Cu^{2+} (Fig. 3b). The EDX spectrographs of ZnFe-LDH before adsorption (Fig. 3a) revealed the presence and percentage composition of the metal ions used in the preparation of LDH such as Fe and Zn while after adsorption the existence of Cu^{2+} ions adsorbed by ZnFe-LDH was expressed in the EDX spectrograph (Fig. 3b). Therefore, from the EDX analyses, it can be concluded that some chemical changes have occurred during the adsorption process. Similarly, the FE-SEM and EDX images of ZnFe-LDH composite with CNTs before and after Cu^{2+} are presented in Figs. 3c and d.

The aggregates or agglomerates of different sizes and the EDX elemental distribution are well pronounced before and after adsorption (Figs. 3c and d) suggesting a successful formation of ZnFe-LDH composite with CNT, and the presence of Cu^{2+} in the elemental analysis provides the evidence of successful adsorption and some chemical changes. Similarly, the FE-SEM and EDX images of ZnFe-LDH composite with OPb before and after adsorption of Cu^{2+} are presented in Figs. 3e and f. Before adsorption, rough and porous surfaces of biochar and ZnFe-LDH

particles were evident in LDH/OPb (Fig. 3e) and the EDX elemental distribution revealed successful synthesis of the composite. Also, in the LDH/OPb sample after Cu^{2+} adsorption (Fig. 3f), the brighter surface of the biochar and some particles can be attributed to Cu^{2+} metal ions adsorption. From the EDX elemental analysis, the presence of Cu^{2+} revealed successful adsorption occurrence.

3.1.3. Equilibrium contact time and optimization of batch parameters

To investigate the influence of contact time on the adsorption of Cu^{2+} and determine the equilibrium contact time, 20, 40, and 60 mg L^{-1} of the initial Cu^{2+} concentrations were chosen with the solution pH and adsorbent dose kept fixed at 5.0 and 0.5 g, respectively. The changes in the sorption capacity and percentage removal of Cu^{2+} by ZnFe-LDH and its composites with CNT and OPb over a contact time of about 3 h are depicted in Fig. 4.

Although there is a continual increase in the adsorption capacity with increasing contact time, insignificant changes ($p = 0.01$) were observed after a contact time of 30 or 60 min for both 20 and 60 mg L^{-1} of Cu^{2+} . For the 20 mg L^{-1} of

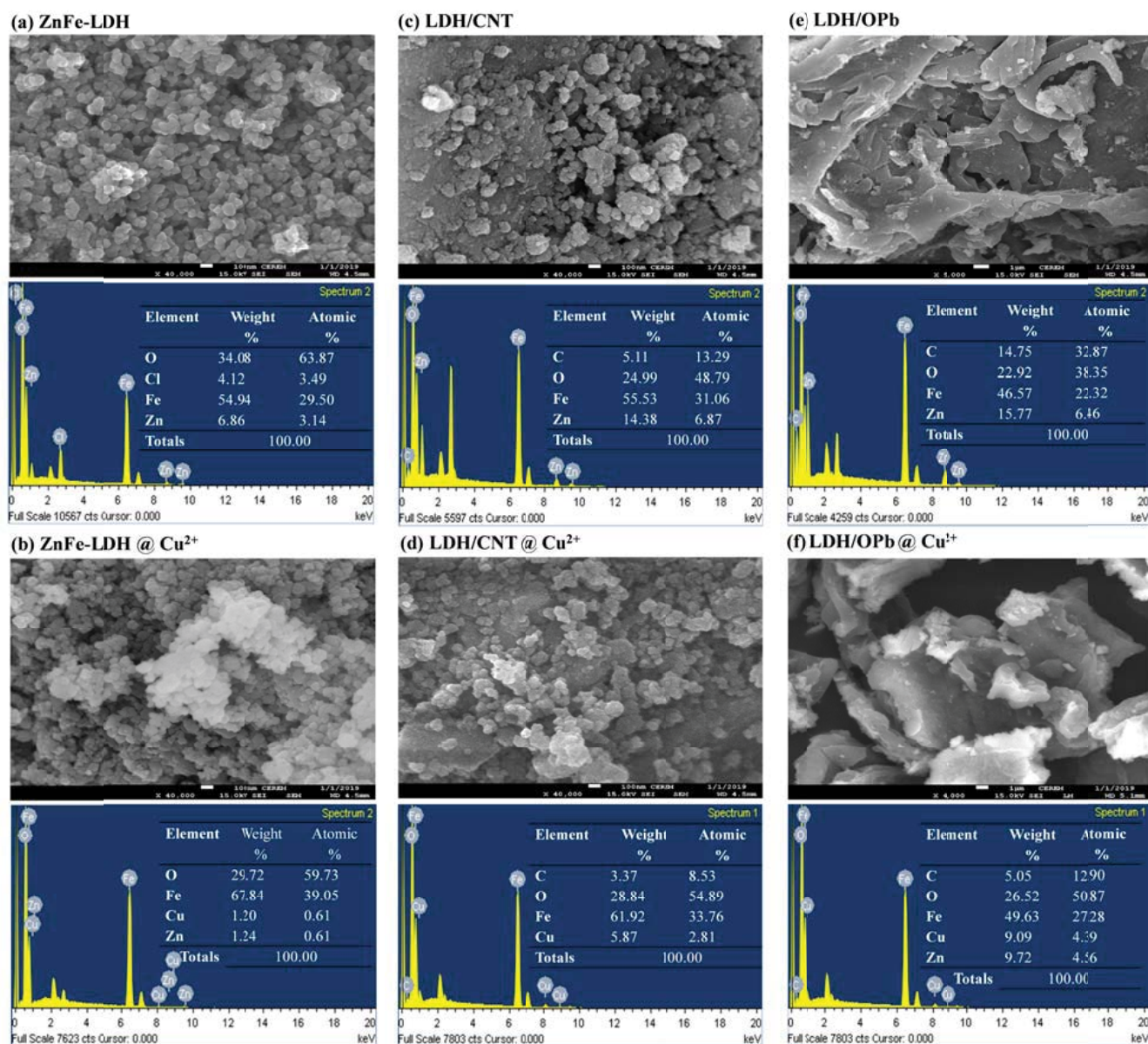


Fig. 3. SEM and EDX images of ZnFe-LDH and its composites before and after the adsorption of Cu²⁺: (a) ZnFe-LDH, (b) ZnFe-LDH@Cu²⁺, (c) LDH/CNT, (d) LDH/CNT@Cu²⁺, (e) LDH/OPb, and (f) LDH/OPb@Cu²⁺.

Cu²⁺, more than 90% removal efficiency was observed when using LDH/OPb while LDH/CNT and ZnFe-LDH exhibited about 65% and 40% removal efficiency, respectively, after a contact time of 1 h. A similar trend was noticed at 60 mg L⁻¹, thus rendering 60 min to be chosen as the equilibrium contact time for the optimum removal of the studied metal with all adsorbents. The quick adsorption of Cu²⁺ during the initial contact with ZnFe-LDH and its composite adsorbents is attributed to the presence of unused active sites on the surface of the adsorbents. LDH/OPb demonstrated greater affinity toward the studied metal than LDH/CNT by almost 20% which in turn exhibited better removal efficiency (almost 20%) than ZnFe-LDH, as shown in Figs. 4a and b. This was probably due to the larger surface area of LDH/OPb (107 m² g⁻¹) than LDH/CNT (81 m² g⁻¹) and

ZnFe-LDH (69 m² g⁻¹). The values of the maximum adsorption capacities obtained using all three adsorbents is presented in Table 1 and compared with various adsorbents used in different studies for the adsorption of Cu²⁺.

To optimize the dose of the adsorbent, an equilibrium contact time of 60 min was adopted, as determined above, while the initial solution pH and Cu²⁺ concentrations were maintained at 5.0 and 20 mg L⁻¹, respectively. The changes in the sorption capacity and removal efficiency of Cu²⁺ were examined by selecting a variable dose of all the adsorbents in the range of 0.2–0.9 g, as depicted in Fig. 5a. From the Fig. 5, different trends were observed for the three adsorbents; insignificant changes in the adsorption capacity of ZnFe-LDH within the dose range while a linear decreasing trend in the adsorption capacity was observed as the

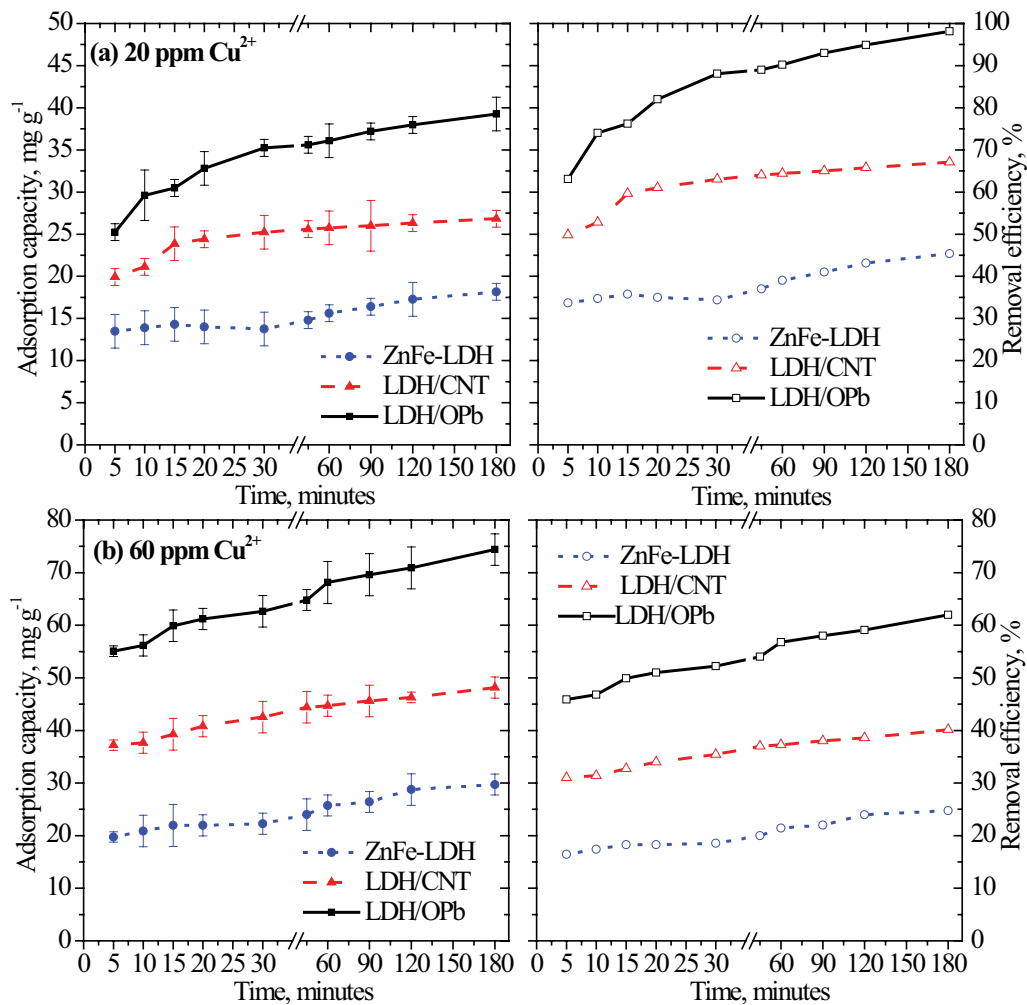


Fig. 4. Variation in the sorption capacity of Cu^{2+} and removal efficiency using ZnFe-LDH and its composites at (a) 20 and (b) $60 \text{ mg L}^{-1} \text{ Cu}^{2+}$.

Table 1
Comparison of adsorption capacities of various adsorbents for Cu^{2+} ions

Type of adsorbent	Maximum adsorption capacity, mg g^{-1}	Reference
ZnFe-LDH	25	This study
LDH/CNT	44	
LDH/OPb	68	
$\text{Mg}_2\text{Al-LS-LDH}$	64	[49]
$\text{MoS}_4\text{-LDH}$	181	[50]
Hydrotalcite modified by tannin (TA-HTC)	81	[51]
Grape bagasse activated carbon	43	[52]
ZnAl-LDH intercalated with EDTA	71	[53]
Activated carbon thorough micro-nano spheres	42	[54]
MgAl-LDH modified palygorskite (Pal/MgAl-LDH)	45	[55]
$\text{SC}_4\text{A-NO}_3\text{-LDH}$	8	[56]
Biochar/MnAl-LDH	74	[57]

dose of LDH/CNT or LDH/OPb varied within the range. The removal efficiency, however, increased linearly for the three adsorbents within the investigated dose range, although insignificant changes were noticed for LDH/CNT and LDH/OPb as their doses increased from 0.5 to 0.9 g. An increase in the dose of adsorbents corresponded to abundant adsorption sites [36,37] which contributed to the increased removal efficiency, while a fixed concentration of Cu^{2+} (20 mg L^{-1}) resulted in an agglomeration of the adsorbent particles as evident from the insignificant changes in the adsorption capacities.

The pH of the solution was optimized by adopting the equilibrium contact time as 60 min, optimum dose of different adsorbents as 0.5 g, and initial metal concentration as 20 mg L^{-1} . Fig. 5b shows the changes in the adsorption capacity and percentage removal of the studied metal using all the adsorbents while performing the batch test in a pH range of 2–5. For the LDH/OPb, exponential changes were observed in both the adsorption capacity and removal efficiency of about 36 mg g^{-1} and 90%, respectively, as the pH increased from 2.0 to 5.0. For ZnFe-LDH and LDH/CNT, there was a linear increase in both the sorption capacity and percentage removal up to a pH of 4 while an exponential increase was observed with a further increase in the pH to 5.0. As shown in Fig. 5b, a two- and three-fold increase in the sorption capacity and removal efficiency of Cu^{2+} were observed in the pH range of 4.0–5.0 compared to the pH range of 2.0–4.0 for LDH/CNT and ZnFe-LDH, respectively. Thus, the effects of the degree of ionization and surface charge on the surface of the adsorbent have been clearly demonstrated with supportive evidence by changes in the adsorption capacity and removal efficiency of Cu^{2+} with varying solution pH [38–40]. The optimum pH value can be considered to be 6 for all the adsorbents or even 5 for LDH/OPb because there is only a minute difference in the sorption capacity or percentage removal between both pH values.

Fig. 5c illustrates the changes in the sorption capacity and removal efficiency within the investigated range of the initial metal concentrations ($10\text{--}100 \text{ mg L}^{-1}$). An equilibrium contact time of 60 min and the optimum values of the adsorbent dose and solution pH of 0.5 g and 5.0, respectively, were adopted for the batch test. As depicted in Fig. 5c, an increasing trend in the sorption capacity was observed for the three adsorbents as the initial Cu^{2+} concentration increased from 10 to 60 mg L^{-1} while a further increase in the initial Cu^{2+} concentration to 100 mg L^{-1} resulted in a decrease of the sorption capacity. The increase in the sorption capacity of LDH/OPb, however, was two- and three-folds higher than ZnFe-LDH and LDH/CNT, respectively, emphasizing the preference for LDH/OPb over LDH/CNT and/or ZnFe-LDH. Similarly, a uniform trend for the three adsorbents was observed concerning the decreased removal efficiency as the initial Cu^{2+} concentration increased from 10 to 100 mg L^{-1} . A decrease in the removal efficiency of about 70% and 40% was noticed in LDH/OPb and ZnFe-LDH, respectively, as the initial Cu^{2+} concentration increased from 10 to 100 mg L^{-1} .

3.2. Two- and three-parameter isotherms models

The adsorption data obtained from the batch experiments were analyzed using two- and three-parameter

isotherm models. The data for the batch experiments were generated for different initial Cu^{2+} concentrations ($10\text{--}100 \text{ mg L}^{-1}$) by maintaining the solution pH and temperature at 5.0°C and 30°C , respectively while 0.5 g of the adsorbent dose was employed for an equilibrium contact time of 60 min. The two-parameter models employed in this study were the Langmuir, Freundlich, and Dubinin–Radushkevich (D–R) isotherms while the three-parameter models included the Freundlich–Langmuir (F–L) and Redlich–Peterson (R–P) isotherms. The correlation coefficient (R^2), maximum adsorption capacity to predict and compare the biosorption performance, and other related parameters were evaluated in each isotherm model and their values are presented in Table 2. Eq. (4) expresses the linearized Langmuir isotherm model, which is suitable for a monolayer adsorption system. C_e (mg L^{-1}) and q_e (mg g^{-1}) are the solution concentration and adsorption capacity of Cu^{2+} at equilibrium, respectively, while q_m (mg g^{-1}) and K_L (L mg^{-1}) are the maximum sorption capacity and Langmuir constant, respectively. The shape of the isotherm was described based on a separation factor R_L $[(1 + K_L C_0)^{-1}]$ [41]. The linearized form of the Freundlich isotherm model, suitable for heterogeneous adsorption systems, is expressed in Eq. (5) with K_F (L g^{-1}) and $1/n$ representing the Freundlich constant and favorability of the adsorption system, respectively [42]. Eq. (6) shows the linearized form of D–R isotherm which is usually suitable for an intermediate range of solvent concentrations with high solute activities [43]. The value of ϵ (a parameter) was evaluated according to Eq. (6a) with R ($8.314 \text{ J mol}^{-1} \text{ K}^{-1}$) and T (Kelvin) being the universal gas constant and absolute temperature, respectively. Furthermore, the slope of the linearized plot ($\ln q_e$ vs. ϵ^2), β , was employed to calculate the mean free energy of adsorption, E (kJ mol^{-1}), according to Eq. (6b), which categorized the adsorption to be either physical ($E < 8 \text{ kJ mol}^{-1}$) or chemical ($E = 8\text{--}16 \text{ kJ mol}^{-1}$).

$$\frac{1}{q_e} = \frac{1}{q_m} + \left(\frac{1}{q_m K_L} \right) \frac{1}{C_e} \quad (4)$$

$$\log q_e = \log K_F + \frac{1}{n} \log C_e \quad (5)$$

$$\ln q_e = \ln q_m - \beta \epsilon^2 \quad (6)$$

$$\epsilon^2 = RT \ln \left(1 + \frac{1}{C_e} \right) \quad (6a)$$

$$E = \frac{1}{\sqrt{2\beta}} \quad (6b)$$

The fitting of the adsorption data of Cu^{2+} (60 mg L^{-1}) onto ZnFe-LDH and its composites for both the Langmuir and Freundlich isotherm models is presented in Figs. 6a and b, respectively. The values of the related constants and parameters in both models were calculated according to the linearized plots of $1/q_e$ vs. $1/C_e$ (Langmuir) and $\log q_e$ vs. $\log C_e$ (Freundlich), and they are presented in Table 2. Relatively higher R^2 values (0.95–0.99) in the Langmuir

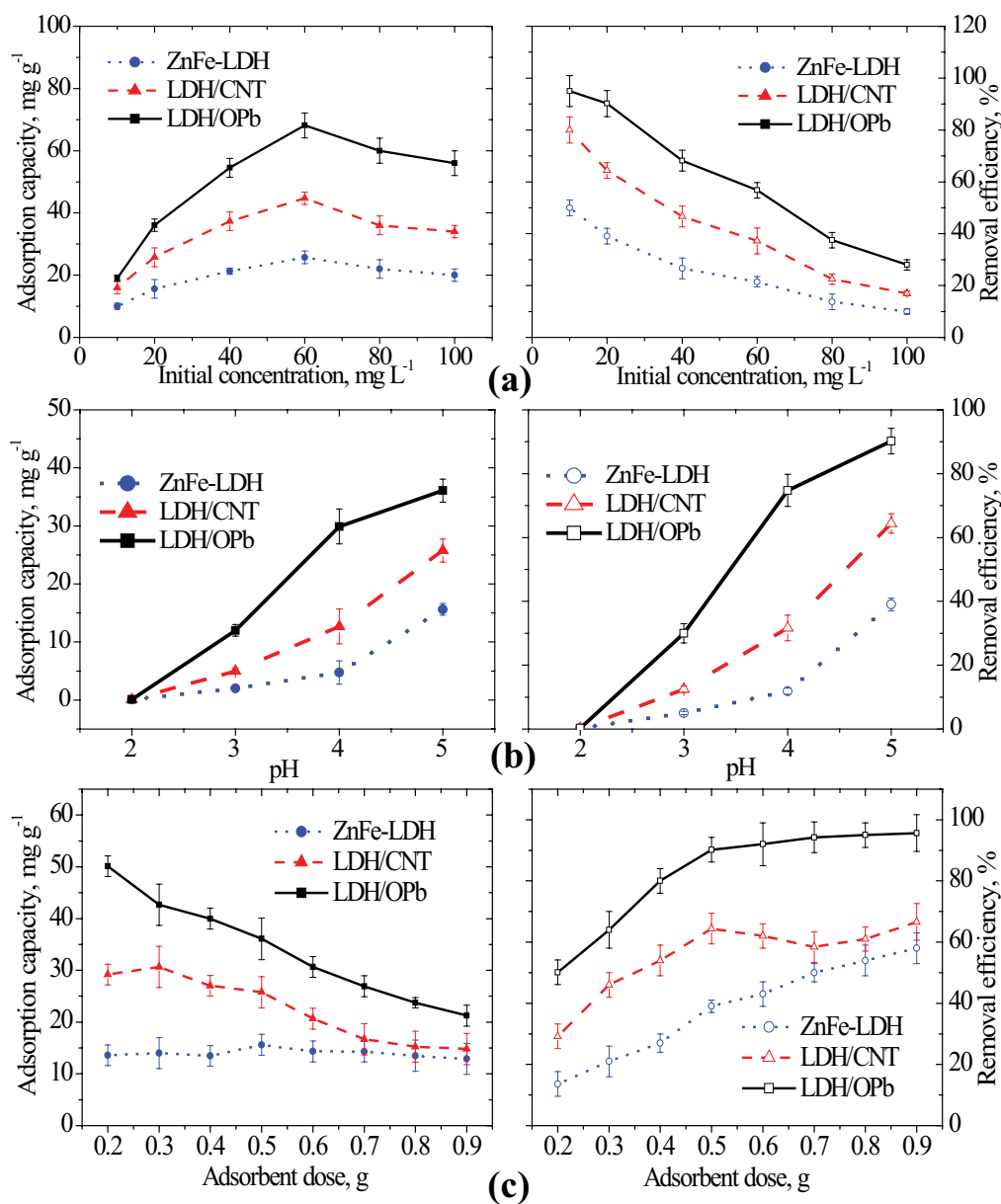


Fig. 5. Variation in the sorption capacity of Cu^{2+} and removal efficiency using ZnFe-LDH and its composites upon changing the (a) initial Cu^{2+} concentration, (b) solution pH, and (c) dose of the adsorbent.

model than the Freundlich isotherm (0.75–0.91) indicated better application of the former to adsorption data than the latter. The highest value of K_L (0.9 L mg^{-1}) was observed for LDH/OPb while the lowest (0.13 L mg^{-1}) was exhibited by ZnFe-LDH, as shown in Table 2. The values of the separation factor, R_L , also lied within the favorable range (0–1) for all adsorbents although the predicted maximum sorption capacity was slightly underestimated for the composite adsorbents (LDH/CNT and LDH/OPb). In the Freundlich isotherm model, LDH/OPb also exhibited the highest value of K_L (32.83 L g^{-1}) while ZnFe-LDH demonstrated the lowest (9.22 L g^{-1}), as shown in Table 2. Although n (3.75–4.46) lied within the favorable range (2–10) in the Freundlich model, the predicted maximum sorption capacity

was overestimated in the experimental values for all the adsorbents (e.g., 82 against 68 mg g^{-1} for LDH/OPb, Table 2).

There was a relatively good fit to the adsorption data of the D–R isotherm model as reflected by high R^2 (0.90–0.97, Table 2). The predicted maximum sorption capacity was slightly less than the experimental value, specifically for the composite adsorbents, as shown in Table 2 (e.g., 61 against 68 mg g^{-1} for LDH/OPb). As indicated by the β values in Table 2, higher adsorption energy was observed for ZnFe-LDH compared with the composite adsorbents, while the highest mean free energy of adsorption, E , was exhibited for LDH/OPb (50 kJ mol^{-1}) with the lowest for ZnFe-LDH ($22.94 \text{ kJ mol}^{-1}$). The studied three-parameter isotherm models, namely the Sips and R–P isotherm

models, combine both the Langmuir and Freundlich isotherms, and they are expressed according to Eqs. (7) and (8), respectively.

$$q_e = \frac{q_m K_S C_e^n}{(1 + K_S C_e^n)} \quad (7)$$

$$q_e = \frac{K_{RP} C_e}{(1 + \alpha C_e^\beta)} \quad (8)$$

In Eq. (7), K_S ($L g^{-1}$) and n (dimensionless) represent the energy of adsorption and degree of heterogeneity, respectively. In Eq. (8), K_{RP} ($L g^{-1}$) represents the R–P constant along with α ($L mg^{-1}$) and β (dimensionless, 0–1) [44,45]. The Sips model perfectly predicts the heterogeneous adsorption systems [43] while the R–P isotherm is suitable for both homogeneous and heterogeneous systems due to its versatility [46]. As shown in Table 2, the R–P isotherm model provided a better interpretation of the adsorption data than the Sips isotherm based on higher R^2 values. In both models, a better representation of the adsorption data was observed for ZnFe-LDH compared to the composite adsorbents. Additionally, ZnFe-LDH exhibited more heterogeneity than LDH/CNT and LDH/OPb based on the highest n values (1.55 for ZnFe-LDH).

3.3. Application of the kinetic models to the adsorption data

To determine the kinetics, three different initial metal concentrations (20, 40, and 60 $mg L^{-1}$) were selected with an

adsorbent (ZnFe-LDH, LDH/CNT, and LDH/OPb) dose of 0.5 g at a solution pH of 5.0. The batch experimental data of Cu^{2+} adsorption by ZnFe-LDH, LDH/CNT, and LDH/OPb were modeled using various kinetic models, namely, the pseudo-first-order (PFO), pseudo-second-order (PSO), intraparticle diffusion, and Elovich kinetic models as presented in Eqs. (9)–(12), respectively.

$$\log(q_e - q_t) = \log q_e - \frac{k_1}{2.303} t \quad (9)$$

$$\frac{t}{q_t} = \frac{1}{k_2 q_e^2} + \frac{1}{q_e} t \quad (10)$$

$$q_t = K_{in} t^{1/2} + C \quad (11)$$

$$q_t = \beta \ln(t) + \beta \ln(\alpha) \quad (12)$$

Eq. (9) is the linearized form of PFO with k_1 (h^{-1}) as the rate constant while Eq. (10) represents the PSO with k_2 as the rate constant ($g mg^{-1} min^{-1}$). The intraparticle diffusion model is expressed in Eq. (11) with K_{in} ($mg g^{-1} min^{1/2}$) as the rate constant while C ($mg g^{-1}$) is a measure of the boundary-layer thickness. The Elovich kinetic model is presented in Eq. (12), where α ($mg g^{-1} min^{-1}$) denotes the initial adsorption rate constant and β ($g mg^{-1}$) the activation energy of chemisorption. Table 3 presents the estimated values of the parameters as calculated from the respective linearized plots.

Table 2
Variables of the two- and three-parameter isotherm models for Cu^{2+} (60 $mg L^{-1}$) adsorption onto LDH and its composites

Isotherm	Parameter	ZnFe-LDH	LDH/CNT	LDH/OPb
Langmuir	$q_{e,exp}$ ($mg g^{-1}$)	25.74	44.7	68.14
	q_{max} ($mg g^{-1}$)	25.38	39.53	60.61
	K_L ($L mg^{-1}$)	0.13	0.34	0.9
	R_L	0.11	1	0.018
	R^2	0.96	0.95	0.99
Freundlich	q_m ($mg g^{-1}$)	27.45	49.62	82.25
	K_F ($L g^{-1}$)	9.22	19.83	32.83
	n	3.75	4.46	4.46
	R^2	0.76	0.75	0.85
Dubinin–Radushkevich	q_m ($mg g^{-1}$)	24.15	39.07	61.08
	β ($mol kJ^{-1}$) ²	0.0039	0.0029	0.0024
	E ($kJ mol^{-1}$)	11.32	13.13	14.43
	R^2	0.91	0.9	0.97
Sips	q_m ($mg g^{-1}$)	23	39	62.48
	K_S ($L mg^{-1}$)	0.058	0.26	0.784
	n	1.55	1.2	0.978
	R^2	0.85	0.82	0.93
Redlich–Peterson	K_{RP} ($L g^{-1}$)	1.9	6.7	40.3
	α ($L mg^{-1}$)	0.0114	0.058	0.535
	β	1.43	1.25	1.05
	R^2	0.92	0.88	0.94

As presented in Table 3, the PFO kinetic model estimated significantly low values of R^2 for the adsorption of Cu^{2+} by the three adsorbents. The unsuitability of PFO kinetic models was further proved by the extremely lower calculated adsorption capacities (not shown) than the experimental adsorption values (Table 3). Fig. 7 shows the application of the PSO kinetic model to the adsorption of Cu^{2+} using different initial Cu^{2+} concentrations (20, 40, and 60 mg L^{-1}) with a solution pH of 5 and adsorbents dose of 0.5 g.

The best fitting of the adsorption data was achieved with the PSO model, as shown in Fig. 7, and was reflected by a high value of R^2 (close to unity). This was true for the three adsorbents with the used initial concentrations of Cu^{2+} . The best-fit of this model was also proved by the close

consistency of the calculated adsorption capacities with the experimental values, though slightly overestimated, as shown in Table 3. The application of this model helped to conclude that the chemisorption is the rate-controlling step during the adsorption of Cu^{2+} . The initial adsorption rate, h , in this model ($k_2 \times q_e^2 \text{ mg g}^{-1} \text{ min}^{-1}$) was also estimated and the highest values were observed for LDH/OPb (at 60 mg L^{-1}) which increased from 9 to 16 $\text{mg g}^{-1} \text{ min}^{-1}$ as the initial Cu^{2+} concentration increased from 20 to 60 mg L^{-1} , as shown in Table 3. Furthermore, ZnFe-LDH possessed the lowest initial adsorption rate (2.7–3.9) while LDH/CNT exhibited the highest h values at 20 and 40 mg L^{-1} (Table 3).

LDH/OPb exhibited the highest values of K_{in} (1–2.5 $\text{mg g}^{-1} \text{ min}^{1/2}$) compared to LDH/CNT and ZnFe-LDH

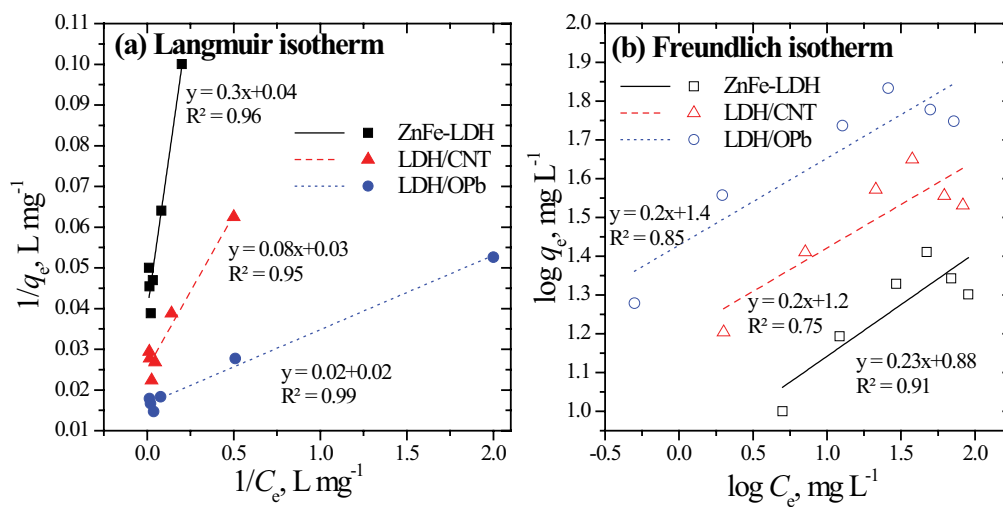


Fig. 6. Fitting of the linearized (a) Langmuir and (b) Freundlich isotherms to the adsorption data of Cu^{2+} (60 mg L^{-1}) onto LDH and its composites.

Table 3
Parameters of the different kinetic models for Cu^{2+} adsorption onto LDH and its composites

Kinetic model	Parameter	Initial Cu^{2+} concentration (mg L^{-1})								
		ZnFe-LDH			LDH/CNT			LDH/OPb		
		20	40	60	20	40	60	20	40	60
PFO	$q_{e,exp}$ (mg g^{-1})	15.62	21.30	25.74	25.76	37.32	44.7	36.08	54.524	68.14
	k_1 (h^{-1})	0.0037	0.0056	0.0108	0.0055	0.0092	0.0113	0.0108	0.0143	0.0164
	R^2	0.42	0.29	0.69	0.0984	0.36	0.36	0.34	0.5	0.72
PSO	$q_{e,cal}$ (mg g^{-1})	18.35	25.77	30.30	27.03	41.84	48.54	39.68	69.93	75.19
	k_2 ($\text{g mg}^{-1} \text{ min}^{-1}$)	0.0081	0.0051	0.0042	0.0152	0.005	0.0055	0.0057	0.0014	0.0028
	h ($\text{mg g}^{-1} \text{ min}^{-1}$)	2.74	3.40	3.897	11.07	8.67	13.05	8.99	6.87	15.798
	R^2	0.9957	0.9911	0.9957	0.9998	0.9966	0.9992	0.9994	0.9863	0.9986
Intraparticle diffusion	K_{in} ($\text{mg g}^{-1} \text{ min}^{1/2}$)	0.4354	0.6871	0.9217	0.5252	0.9578	0.9971	1.0848	2.5006	1.7316
	C (mg g^{-1})	12.226	16.173	17.916	20.958	29.372	35.929	26.622	35.949	52.585
	R^2	0.95	0.96	0.98	0.7	0.85	0.92	0.81	0.93	0.96
Elovich	α ($\text{mg g}^{-1} \text{ min}^{-1}$)	3,477	533	136	15,118	2,404	14,075	276	23	3,386
	β (g mg^{-1})	1.30	2.12	2.85	1.86	3.16	3.26	3.70	7.80	5.50
	R^2	0.83	0.91	0.93	0.87	0.93	0.97	0.95	0.94	0.95

while the lowest values (0.4–0.9) were observed for the simple ZnFe-LDH (Table 3) with the lowest R^2 values (0.7 at 20 mg L⁻¹ of Cu²⁺). The thickness of the boundary layer was also higher in LDH/OPb (27–52 mg g⁻¹) while the lowest values (12–18 mg g⁻¹) were observed in ZnFe-LDH, as shown in Table 3. High R^2 (>0.9 except for LDH/CNT and ZnFe-LDH at 20 mg L⁻¹ of Cu²⁺) indicated a good fit of the Elovich model to the experimental data. The initial adsorption rate was highest in LDH/OPb while the lowest was displayed in ZnFe-LDH, as shown in Table 3. A reverse trend was noticed for β with the highest values in ZnFe-LDH (3.7–7.8 g mg⁻¹, Table 3) and the lowest values and extent of surface coverage observed in LDH/OPb (1.3–2.85 g mg⁻¹). Hence, the chemisorption onto the adsorbents' surface with heterogeneous nature was accurately proposed with the multistep adsorption mechanism and dominating intraparticle diffusion [47,48].

4. Conclusions

In this study, ZnFe-LDH and its composites with single-wall CNTs and biochar derived from OPb were

synthesized successfully using a co-precipitation method. The XRD patterns indicated that ZnFe-LDH exhibited better crystallinity than the composite adsorbents, which demonstrated amorphous nature and changes in intensity due to the formation of new compounds after Cu²⁺ adsorption. The aggregates or agglomerates of different sizes and the EDX elemental distribution before and after adsorption suggested the successful formation of ZnFe-LDH composite with CNT. The brighter surface of the biochar and some particles can be attributed to Cu²⁺ adsorption as shown by the FE-SEM and EDX images of ZnFe-LDH composite with OPb.

There was a continual increase in the adsorption capacity and removal efficiency with increasing contact time and 60 min was adopted as the equilibrium contact time for the optimum removal of the studied metal by all the adsorbents. LDH/OPb demonstrated a greater affinity for the studied metal than LDH/CNT and ZnFe-LDH due to its larger surface area (107 m² g⁻¹) than LDH/CNT (81 m² g⁻¹) and ZnFe-LDH (69 m² g⁻¹). A linear decreasing trend in the adsorption capacity was observed as the dose of LDH/CNT or LDH/OPb increased from 0.2 to 0.9 g.

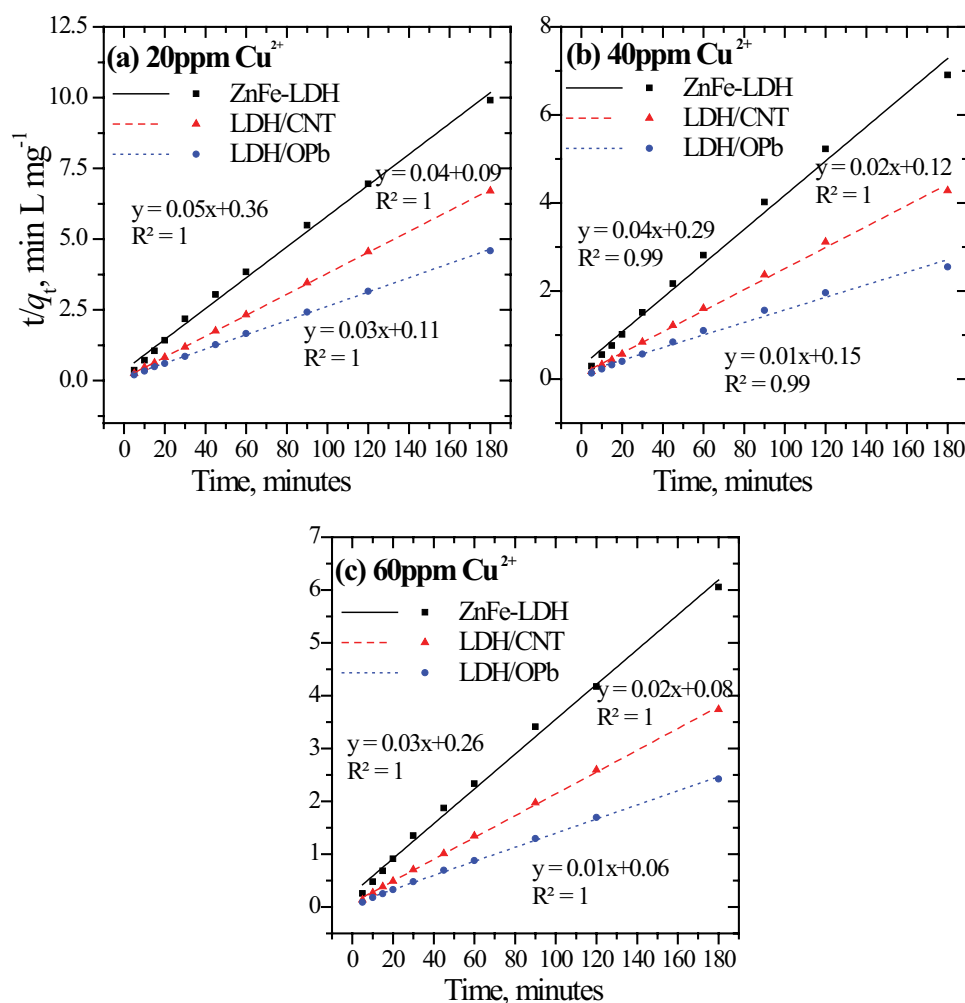


Fig. 7. Fitting of the PSO kinetic model to various initial solution concentrations of Cu²⁺ using LDH and its composites: (a) 20, (b) 40, and (c) 60 ppm Cu²⁺.

A two- and three-fold increase in the sorption capacity and removal efficiency of Cu^{2+} were observed in the pH range of 4.0–5.0 compared to the pH range of 2.0–4.0 for LDH/CNT and ZnFe-LDH, respectively. The optimum pH value was considered to be 6.0 (for all adsorbents) or 5.0 (for LDH/OPb). The increase in sorption capacity, by increasing the initial Cu^{2+} concentration from 10 to 60 mg L^{-1} , was two- and three-folds higher for LDH/OPb than ZnFe-LDH and LDH/CNT, respectively, emphasizing the preference for LDH/OPb over LDH/CNT and/or ZnFe-LDH.

The relatively higher R^2 values (0.95–0.99) in the Langmuir model than the Freundlich isotherm (0.75–0.91) suggested a better application of the former to the adsorption data compared with the latter. The D–R isotherm presented a reasonable good fit to the adsorption data with the highest mean free energy of adsorption for LDH/OPb. A good representation of the adsorption data was realized for ZnFe-LDH compared to the composite adsorbents in both three-parameter isotherm models. Among the kinetic models, the PFO presented a poor representation of the adsorption data while the best fitting of the adsorption data was demonstrated by the PSO model, as indicated by the high value of R^2 (close to unity), thus, helping to conclude that the chemisorption is the rate-controlling step for the adsorption of Cu^{2+} . The application of the Elovich kinetic model suggested the heterogeneous nature of the adsorbents' surface with a multistep adsorption mechanism involving the chemisorption and dominating intraparticle diffusion.

Acknowledgments

This project was funded by the National Plan for Science, Technology and Innovation (MAARIFAH), King Abdulaziz City for Science and Technology, Kingdom of Saudi Arabia, Award Number (12-WAT2623-02). The authors appreciate the Deanship of Scientific Research and RSSU at King Saud University for their technical support (manuscript editing services).

References

- J.C. Igwe, A.A. Abia, A bioseparation process for removing heavy metals from waste water using biosorbents, *Afr. J. Biotechnol.*, 5 (2006) 1167–1179.
- N. Ayawei, T. Ekubo, D. Wankasi, D. Dikio, Synthesis and application of layered double hydroxide for the removal of copper in wastewater, *Int. J. Chem.*, 7 (2015) 122–132.
- M. Bilal, J.A. Shah, T. Ashfaq, S.M.H. Gardazi, A.A. Tahir, A. Pervez, H. Haroon, Q. Mahmood, Waste biomass adsorbents for copper removal from industrial wastewater—a review, *J. Hazard. Mater.*, 263 (2013) 322–333.
- M. Shafiq, A.A. Alazba, M.T. Amin, Removal of heavy metals from wastewater using date palm as a biosorbent: a comparative review, *Sains Malaysiana*, 47 (2018) 35–49.
- F. Fu, Q. Wang, Removal of heavy metal ions from wastewaters: a review, *J. Environ. Manage.*, 92 (2011) 407–418.
- R. Shan, L. Yan, K. Yang, Y. Hao, B. Du, Adsorption of Cd(II) by Mg–Al– CO_3 - and magnetic Fe_3O_4 /Mg–Al– CO_3 -layered double hydroxides: kinetic, isothermal, thermodynamic and mechanistic studies, *J. Hazard. Mater.*, 299 (2015) 42–49.
- M.T. Amin, A.A. Alazba, M. Shafiq, Application of biochar derived from date palm biomass for removal of lead and copper ions in a batch reactor: kinetics and isotherm scrutiny, *Chem. Phys. Lett.*, 722 (2019) 64–73.
- M. Guo, G. Qiu, W. Song, Poultry litter-based activated carbon for removing heavy metal ions in water, *Waste Manage.*, 30 (2010) 308–315.
- A.A. Bakr, M.S. Mostafa, E.A. Sultan, Mn(II) removal from aqueous solutions by Co/Mo layered double hydroxide: kinetics and thermodynamics, *Egypt. J. Pet.*, 25 (2016) 171–181.
- S. Zhang, F. Cheng, Z. Tao, F. Gao, J. Chen, Removal of nickel ions from wastewater by $\text{Mg}(\text{OH})_2$ /MgO nanostructures embedded in Al_2O_3 membranes, *J. Alloys Compd.*, 426 (2006) 281–285.
- K. Abderrazek, F.S. Najoua, E. Srasra, Synthesis and characterization of [Zn–Al] LDH: study of the effect of calcination on the photocatalytic activity, *Appl. Clay Sci.*, 119 (2016) 229–235.
- M.C. Richardson, P.S. Braterman, Cation exchange by anion-exchanging clays: the effects of particle aging, *J. Mater. Chem.*, 19 (2009) 7965–7975.
- J. Sun, Y. Chen, H. Yu, L. Yan, B. Du, Z. Pei, Removal of Cu^{2+} , Cd^{2+} and Pb^{2+} from aqueous solutions by magnetic alginate microsphere based on Fe_3O_4 /MgAl-layered double hydroxide, *J. Colloid Interface Sci.*, 532 (2018) 474–484.
- X. Yue, W. Liu, Z. Chen, Z. Lin, Simultaneous removal of Cu(II) and Cr(VI) by Mg–Al–Cl layered double hydroxide and mechanism insight, *J. Environ. Sci. China*, 53 (2017) 16–26.
- M. Inyang, B. Gao, Y. Yao, Y. Xue, A. Zimmerman, A. Mosa, P. Pullammanappallil, Y.S. Ok, X. Cao, A review of biochar as a low-cost adsorbent for aqueous heavy metal removal, *Crit. Rev. Environ. Sci. Technol.*, 46 (2016) 406–433.
- N.A. Sagar, S. Pareek, S. Sharma, E.M. Yahia, M.G. Lobo, Fruit and vegetable waste: bioactive compounds, their extraction, and possible utilization, *Compr. Rev. Food Sci. Food Saf.*, 17 (2018) 512–531.
- P.D. Pathak, S.A. Mandavgane, B.D. Kulkarni, Fruit peel waste: characterization and its potential uses, *Curr. Sci.*, 113 (2017) 444–454.
- P.E.D. Dikio, A. Nimibofa, Adsorption dynamics of copper(II) on Zn/Fe layered double hydroxide, *Eur. J. Sci. Res.*, 130 (2015) 235–248.
- M. Zhang, B. Gao, J. Fang, A.E. Creamer, J.L. Ullman, Self-assembly of needle-like layered double hydroxide (LDH) nanocrystals on hydrochar: characterization and phosphate removal ability, *RSC Adv.*, 4 (2014) 28171–28175.
- R. Soltani, A. Marjani, S. Shirazian, A hierarchical LDH/MOF nanocomposite: single, simultaneous and consecutive adsorption of a reactive dye and Cr(VI), *Dalton Trans.*, 49 (2020) 5323–5335.
- K.M. Parida, L. Mohapatra, Carbonate intercalated Zn/Fe layered double hydroxide: a novel photocatalyst for the enhanced photo degradation of azo dyes, *Chem. Eng. J.*, 179 (2012) 131–139.
- Y. Jiang, Z. Hao, H. Luo, Z. Shao, Q. Yu, M. Sun, Y. Ke, Y. Chen, Synergistic effects of boron-doped silicone resin and a layered double hydroxide modified with sodium dodecyl benzenesulfonate for enhancing the flame retardancy of polycarbonate, *RSC Adv.*, 8 (2018) 11078–11086.
- J.O. Eniola, R. Kumar, O.A. Mohamed, A.A. Al-Rashdi, M.A. Barakat, Synthesis and characterization of CuFe_2O_4 /NiMgAl-LDH composite for the efficient removal of oxytetracycline antibiotic, *J. Saudi Chem. Soc.*, 24 (2020) 139–150.
- G.G.C. Arizaga, J.E.F.d.C. Gardolinski, W.H. Schreiner, F. Wypych, Intercalation of an oxalatoxonobate complex into layered double hydroxide and layered zinc hydroxide nitrate, *J. Colloid Interface Sci.*, 330 (2009) 352–358.
- S. Petit, D. Righi, J. Madejová, Infrared spectroscopy of NH_4^+ -bearing and saturated clay minerals: a review of the study of layer charge, *Appl. Clay Sci.*, 34 (2006) 22–30.
- M. Dinari, A. Nabiyan, Citric acid-modified layered double hydroxides as a green reinforcing agent for improving thermal and mechanical properties of poly(vinyl alcohol)-based nanocomposite films, *Polym. Compos.*, 38 (2017) E128–E136.
- Q. Yang, S. Wang, F. Chen, K. Luo, J. Sun, C. Gong, F. Yao, X. Wang, J. Wu, X. Li, D. Wang, G. Zeng, Enhanced visible-light-driven photocatalytic removal of refractory pollutants

- by Zn/Fe mixed metal oxide derived from layered double hydroxide, *Catal. Commun.*, 99 (2017) 15–19.
- [28] D. Huang, B. Li, M. Wu, S. Kuga, Y. Huang, Graphene oxide-based Fe–Mg (hydr)oxide nanocomposite as heavy metals adsorbent, *J. Chem. Eng. Data*, 63 (2018) 2097–2105.
- [29] N. Tian, X. Tian, X. Liu, Z. Zhou, C. Yang, L. Ma, C. Tian, Y. Li, Y. Wang, Facile synthesis of hierarchical dendrite-like structure iron layered double hydroxide nanohybrids for effective arsenic removal, *Chem. Commun.*, 52 (2016) 11955–11958.
- [30] H. Kowsari, M. Mehrpooya, F. Pourfayaz, Nitrogen and sulfur doped ZnAl layered double hydroxide/reduced graphene oxide as an efficient nanoelectrocatalyst for oxygen reduction reactions, *Int. J. Hydrogen Energy*, 45 (2020) 27129–27144.
- [31] H. Abdolmohammad-Zadeh, K. Tavarid, Z. Talieb, Determination of iodate in food, environmental, and biological samples after solid-phase extraction with Ni–Al–Zr ternary layered double hydroxide as a nanosorbent, *Sci. World J.*, 2012 (2012) 145482 (1–8), doi: 10.1100/2012/145482.
- [32] J.T. Klopogge, L. Hickey, R.L. Frost, FT-Raman and FT-IR spectroscopic study of synthetic Mg/Zn/Al-hydrotalcites, *J. Raman Spectrosc.*, 35 (2004) 967–974.
- [33] X. Tan, Y. Liu, Y. Gu, Y. Xu, G. Zeng, X. Hu, S. Liu, X. Wang, S. Liu, J. Li, Biochar-based nano-composites for the decontamination of wastewater: a review, *Bioresour. Technol.*, 212 (2016) 318–333.
- [34] N.I. Blaisi, M. Zubair, Ihsanullah, S. Ali, T.S. Kazeem, M.S. Manzar, W. Al-Kutti, M.A. Al Harthi, Date palm ash-MgAl-layered double hydroxide composite: sustainable adsorbent for effective removal of methyl orange and eriochrome black-T from aqueous phase, *Environ. Sci. Pollut. Res.*, 25 (2018) 34319–34331.
- [35] W. Yang, Y. Kim, P.K.T. Liu, M. Sahimi, T.T. Tsotsis, A study by *in situ* techniques of the thermal evolution of the structure of a Mg–Al–CO₃ layered double hydroxide, *Chem. Eng. Sci.*, 57 (2002) 2945–2953.
- [36] X.-Y. Huang, X.-Y. Mao, H.-T. Bu, X.-Y. Yu, G.-B. Jiang, M.-H. Zeng, Chemical modification of chitosan by tetraethylenepentamine and adsorption study for anionic dye removal, *Carbohydr. Res.*, 346 (2011) 1232–1240.
- [37] N. Barka, S. Qourzal, A. Assabbane, A. Nounah, Y. Ait-ichou, Removal of Reactive Yellow 84 from aqueous solutions by adsorption onto hydroxyapatite, *J. Saudi Chem. Soc.*, 15 (2011) 263–267.
- [38] M.M. Areco, M.d.S. Afonso, Copper, zinc, cadmium and lead biosorption by *Gymnogongrus torulosus* thermodynamics and kinetics studies, *Colloids Surf., B*, 81 (2010) 620–628.
- [39] D.W. O'Connell, C. Birkinshaw, T.F. O'Dwyer, Heavy metal adsorbents prepared from the modification of cellulose: a review, *Bioresour. Technol.*, 99 (2008) 6709–6724.
- [40] M.A. Al-Ghouti, J. Li, Y. Salamh, N. Al-Laqtah, G. Walker, M.N.M. Ahmad, Adsorption mechanisms of removing heavy metals and dyes from aqueous solution using date pits solid adsorbent, *J. Hazard. Mater.*, 176 (2010) 510–520.
- [41] K.Y. Foo, B.H. Hameed, Preparation, characterization and evaluation of adsorptive properties of orange peel based activated carbon via microwave induced K₂CO₃ activation, *Bioresour. Technol.*, 104 (2012) 679–686.
- [42] P.K. Malik, Use of activated carbons prepared from sawdust and rice-husk for adsorption of acid dyes: a case study of Acid Yellow 36, *Dyes Pigm.*, 56 (2003) 239–249.
- [43] A. Günay, E. Arslankaya, İ. Tosun, Lead removal from aqueous solution by natural and pretreated clinoptilolite: adsorption equilibrium and kinetics, *J. Hazard. Mater.*, 146 (2007) 362–371.
- [44] M. Abtahi, A. Mesdaghinia, R. Saeedi, S. Nazmara, Biosorption of As(III) and As(V) from aqueous solutions by brown macroalga *Colpomenia sinuosa* biomass: kinetic and equilibrium studies, *Desal. Water Treat.*, 51 (2013) 3224–3232.
- [45] K. Naddafi, N. Rastkari, R. Nabizadeh, R. Saeedi, M. Gholami, M. Sarkhosh, Adsorption of 2,4,6-trichlorophenol from aqueous solutions by a surfactant-modified zeolitic tuff: batch and continuous studies, *Desal. Water Treat.*, 57 (2016) 5789–5799.
- [46] F. Gimbert, N. Morin-Crini, F. Renault, P.-M. Badot, G. Crini, Adsorption isotherm models for dye removal by cationized starch-based material in a single component system: error analysis, *J. Hazard. Mater.*, 157 (2008) 34–46.
- [47] Y. Li, Q. Du, T. Liu, J. Sun, Y. Jiao, Y. Xia, L. Xia, Z. Wang, W. Zhang, K. Wang, H. Zhu, D. Wu, Equilibrium, kinetic and thermodynamic studies on the adsorption of phenol onto graphene, *Mater. Res. Bull.*, 47 (2012) 1898–1904.
- [48] K.V. Kumar, A. Kumaran, Removal of methylene blue by mango seed kernel powder, *Biochem. Eng. J.*, 27 (2005) 83–93.
- [49] G. Huang, D. Wang, S. Ma, J. Chen, L. Jiang, P. Wang, A new, low-cost adsorbent: preparation, characterization, and adsorption behavior of Pb(II) and Cu(II), *J. Colloid Interface Sci.*, 445 (2015) 294–302.
- [50] L. Ma, Q. Wang, S.M. Islam, Y. Liu, S. Ma, M.G. Kanatzidis, Highly selective and efficient removal of heavy metals by layered double hydroxide intercalated with the MoS₄²⁻ ion, *J. Am. Chem. Soc.*, 138 (2016) 2858–2866.
- [51] T.S. Anirudhan, P.S. Suchithra, Synthesis and characterization of tannin-immobilized hydrotalcite as a potential adsorbent of heavy metal ions in effluent treatments, *Appl. Clay Sci.*, 42 (2008) 214–223.
- [52] H. Demiral, C. Güngör, Adsorption of copper(II) from aqueous solutions on activated carbon prepared from grape bagasse, *J. Cleaner Prod.*, 124 (2016) 103–113.
- [53] M.R. Pérez, I. Pavlovic, C. Barriga, J. Cornejo, M.C. Hermosín, M.A. Ulibarri, Uptake of Cu²⁺, Cd²⁺ and Pb²⁺ on Zn–Al layered double hydroxide intercalated with EDTA, *Appl. Clay Sci.*, 32 (2006) 245–251.
- [54] F.-C. Huang, C.-K. Lee, Y.-L. Han, W.-C. Chao, H.-P. Chao, Preparation of activated carbon using micro-nano carbon spheres through chemical activation, *J. Taiwan Inst. Chem. Eng.*, 45 (2014) 2805–2812.
- [55] F. Yang, S. Sun, X. Chen, Y. Chang, F. Zha, Z. Lei, Mg–Al layered double hydroxides modified clay adsorbents for efficient removal of Pb²⁺, Cu²⁺ and Ni²⁺ from water, *Appl. Clay Sci.*, 123 (2016) 134–140.
- [56] A.T. Reda, D. Zhang, Sorption of metal ions from aqueous solution by sulfonated calix[4]arene intercalated with layered double hydroxide, *J. Environ. Chem. Eng.*, 7 (2019) 103021 (1–10), doi: 10.1016/j.jece.2019.103021.
- [57] T. Wang, C. Li, C. Wang, H. Wang, Biochar/MnAl-LDH composites for Cu(II) removal from aqueous solution, *Colloids Surf., A*, 538 (2018) 443–450.